Journal of Applied Physics

Electronic properties of CaF_2 bulk and interfaces

Cite as: J. Appl. Phys. **131**, 215302 (2022); https://doi.org/10.1063/5.0087914
Submitted: 10 February 2022 • Accepted: 16 May 2022 • Published Online: 02 June 2022

Jiaqi Chen, Zhaofu Zhang, Yuzheng Guo, et al.

Journal of Applied Physics ARTICLE scitation.org/journal/jap

Electronic properties of CaF_2 bulk and interfaces

Cite as: J. Appl. Phys. **131**, 215302 (2022); doi: 10.1063/5.0087914
Submitted: 10 February 2022 · Accepted: 16 May 2022 ·
Published Online: 2 June 2022

Jiaqi Chen,[1] Zhaofu Zhang,[1,a)] Yuzheng Guo,[2] and John Robertson[1]

AFFILIATIONS

[1]Department of Engineering, Cambridge University, Cambridge CB2 1PZ, United Kingdom
[2]College of Engineering, Swansea University, Swansea SA1 8EN, United Kingdom

[a)]**Author to whom correspondence should be addressed:** zz389@cam.ac.uk

ABSTRACT

The electronic band structures of ultra-wide gap CaF_2 are investigated with both the hybrid functional and the efficient generalized gradient approximation (GGA) + U scheme. The hybrid functional scheme is in excellent agreement with experiments, while introducing an on-site Coulomb interaction to F-2p orbitals also accurately reproduces the experimental bandgap and greatly improves the previous theoretical results using advanced electronic structure schemes. We also apply the GGA + U method to study CaF_2/Si and metal/CaF_2 interfaces. The CaF_2/Si insulating interfaces with a clear bandgap are built based on the electron counting rule. Our supercell calculations of the CaF_2/Si interfaces show a type-II band alignment and the valence band offset follows a descending trend from (001) to (111) then to (110). The calculation convergence of GGA + U is further tested with the metallic contacts. The metal/CaF_2 interfaces are observed to be weakly pinned and different orientations of CaF_2 sharing a similar pinning factor S up to ~0.9, owing to the highly ionic nature of CaF_2. The GGA + U approach is proven to be a useful tool in studying such fluoride interfaces and contacts.

I. INTRODUCTION

Calcium fluoride (CaF_2) is a well-known face-centered-cubic (FCC) crystal with an ultra-wide bandgap (~11.8 eV) and a relatively high dielectric constant (~8.43). Its interesting luminescent properties contribute to its potential application in bioimaging.[1] The considerable progress achieved recently in molecular beam epitaxy (MBE) growth of thin CaF_2 layers also makes it a possible gate insulator in 2D materials-based FETs.[2] Additionally, CaF_2 was introduced as an insulation layer between the Schottky contact and a high-quality InGaN film in metal–semiconductor–metal (MSM) structures.[3] Therefore, it is important to precisely model the heterostructures between CaF_2 and different metal/semiconductor materials to understand the interface properties in a microscopic approach.

The accurate theoretical description of such semiconductor heterostructures or metal contacts requires appropriate prediction of bandgaps of the involved materials and the determination of their band alignment at the interface.[4] However, the calculation of these quantities using density functional theory (DFT) with a local [local density approximation (LDA)] or semilocal generalized gradient approximation (GGA) exchange-correlation (XC) functional approximation suffers from a severe bandgap underestimation. The improper treatment of electron self-interaction can give errors when describing the electron and hole states. The case of CaF_2 is unusual due to the occurrence of both localized and delocalized electronic states. At its lower conduction band (CB), we observe the hybridization of the delocalized Ca 4s and F 3s states and the localized Ca 3d states, which makes the description of the CB a difficult task.

There are advanced methods developed to overcome this deficiency. The GW method,[5] based on Green's function, calculates quasiparticle energies from an expansion of electron self-energies and the dielectric function. This method could correct the bandgap error. However, it is computationally inefficient and not suitable for large supercells. Precise description of Ca 3d states at the CB needs special treatment of the Ca 3s and 3p semicore states as valence states,[6–8] which leads to a significant increase in numerical demand, even for bulk calculations. A second method is hybrid functional calculations, like the screened exchange (sX)[9] or Heyd–Scuseria–Ernerzhof (HSE)[10] functionals. They are less computationally intensive and have been demonstrated to be successful in treating most of the semiconductors and related heterostructures. However, the applicability of such approach to wide gap materials remains unsolved, and there have been insufficient studies regarding the case of CaF_2.[11] Furthermore, the addition of HF exchange can cause a divergence at Fermi energy with metallic systems, such as for Schottky barriers or metallic grain boundaries.[12]

A third method is the GGA + U. It was first introduced to deal with electron–electron repulsion within transition metal and rare earth compounds,[13] where the Hubbard parameter U was added to open-shell metal d states. This method was later extended to closed-shell transition metal compounds like ZnO, TiO_2, and Cu_2O.[14,15] However, unphysically large U values are always needed to correct the bandgap values. It was then noted that combinations of moderate U values on both metal d states and oxygen p states can open up the bandgap.[16,17] Our recent studies have demonstrated that a U term added to only the O-2p states without any d states being involved can reproduce the band structures of oxides like MgO.[17] Overall, GGA + U is considered as a good alternative method of electronic structure correction with both the speed of traditional LDA and GGA methods and the accuracy of hybrid functionals. However, introducing the U term in HfO_2 led to an over-estimate of the electron affinity,[16] although not in MgO.[17] Here, we apply this scheme to the similar ionic CaF_2 system.

Since the band-edge levels from periodic bulk calculations cannot be directly compared with experimental references, it is necessary to examine the accuracy of the theoretical schemes in predicting ionization potentials at the surface and band offsets at interfaces.[18] The validation of the theoretical values against experimental data requires realistic interface supercell slab models taking detailed surface reconstruction or specific interface bondings into consideration.

The CaF_2/Si interface is a prime test case for this purpose. CaF_2 has a closely matched lattice constant (5.46 Å) with silicon (5.43 Å), which allows high-quality CaF_2 layers to be grown on silicon or germanium substrates using MBE.[19] The bandgap of CaF_2 is much larger than that of silicon, which leads to sizable band offsets, thus a challenge for accurate calculation with traditional DFT methods. Substantial reports on structural[20–22] and electronic[20,23–27] properties of the CaF_2/Si(111) interface are available and act as experimental references for the accuracy of calculations. Additionally, we also modelled the CaF_2/Si(001) and CaF_2/Si(110) interfaces.

Being considered as an important class of super ionic crystal,[28] CaF_2 forms weakly interacting interfaces with metals following the Schottky–Mott rule. The degree of Fermi-level pinning of such interfaces should reach the Schottky limit and give a near-unity pinning factor S [$S = \partial\varphi/\partial\Phi_M$, where φ is the Schottky barrier height (SBH) and Φ_M is the metal work function].[29,30] Currently, there are limited reports on metal/CaF_2 interfaces.

The aim of this work is to compare the detailed CaF_2 band structure calculated with different schemes, considering its seriously underestimated bandgap using GGA. We apply the sX and the GGA + U approaches, in the pursuit of developing a full picture of the electronic properties of this material. We also modelled the CaF_2/Si and metal/CaF_2 interfaces to determine the band offsets and SBHs by the beneficial GGA + U method. This work will be a supplement to the understanding of the accuracy of different electronic structure schemes in comparison to the experimental characterization behavior of CaF_2. Meanwhile, it will also fill the gap of theoretical data on the interface electronic properties for these attractive interfaces. Our detailed analysis demonstrates the validity of the sX approach in wide gap materials and proves that the GGA + U approach is not only suitable for alkaline earth oxides like MgO, but also applicable for fluorides.

II. CALCULATION METHODS

The calculations use the CASTEP code,[31] with the plane-wave pseudopotential method and the Perdew–Burke–Ernzerhof version of the generalized gradient approximation (GGA-PBE) for the exchange-correlation functional. Ultra-soft pseudopotentials with a plane-wave cutoff energy of 400 eV are adopted. Energies are converged to below 10^{-6} eV per atom and forces below 10^{-3} eV/Å. A dense $11 \times 11 \times 11$ k-point mesh is used for the Si primitive cell to include the conduction band minimum (CBM), which is not located at high-symmetry k points, and a $7 \times 7 \times 7$ k-point mesh is used for the CaF_2 primitive cell.

The interface supercell consists of ∼20 Å of CaF_2 and ∼20 Å of Si with no vacuum layer for all the orientations considered. The band offsets and SBHs are extracted using the core-level method[32,33] to increase the precision in determining the valence band maximum (VBM) using

$$\Delta E_V = (E^{int}_{core-A} - E^{int}_{core-B}) + (\Delta V_A - \Delta V_B), \quad (1)$$

$$\phi_p = E^{int}_{core} + \Delta V - E_F. \quad (2)$$

The energy difference between the core-level state and VBM is assumed to maintain a constant value in different environments. E^{int}_{core} is the core level state in the interfacial model, ΔV is the energy difference between the core-level state and VBM of the bulk materials, and E_F is the metal work function. The semi-core 2s state of F atom away from the interface region is chosen as the reference core-level state here.

III. RESULTS AND DISCUSSION

A. Bandgaps and band-edge levels of bulk materials

The results for the detailed band structures of CaF_2 calculated with different methods are shown in Fig. 1. The energies of these levels at high-symmetry points (Γ, X, and L) are given in Table I. CaF_2 has an indirect bandgap, as shown in Fig. 1. The highest valence band (VB) state is at X, and the lowest CB state is at Γ. The VB top originates mainly from F 2p orbitals with only very small contributions from Ca [Fig. 1(a) right panel]. The presence of two F atoms in a unit cell gives rise to two distinct VB levels at the Γ point. The phase reversal that occurs between two translation-related atoms transforms the bonding conditions between F p_x orbitals to a totally antibonding/bonding states at the X point. As a result, the X_2' state lies above Γ_{15} and becomes the VBM.

The lower CB is mostly dominated by Ca 3d orbitals, except for the lowest energy state at Γ. The Γ_1 state consists of delocalized Ca 4s and F 3s orbitals, resulting in the formation of a highly dispersive band. Figure 1(a) right panel indicates that the tail of the DOS at the bottom of the CB is of s-type character. The upper Γ_{12} and Γ_{25}' states are composed of the localized Ca 3d state, with a small mixture of F p at the Γ_{25}' state, which leads to several flatbands.

The implementation of sX pushes up the CB and results in a significantly wider bandgap compared to the GGA method, with the direct gap (Γ−Γ) and the indirect gap (X−Γ) being 12.04 and 11.78 eV, respectively. The sX gap is close to the experimental value

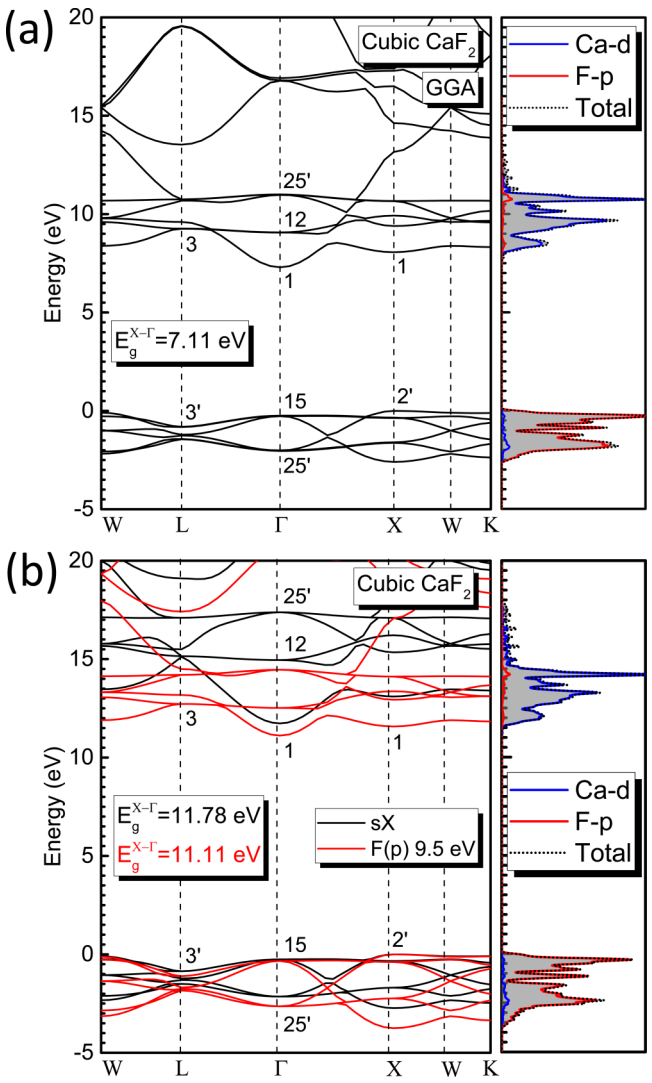

FIG. 1. Calculated band structures and partial density of states (PDOS) of CaF_2 with (a) GGA functional and (b) sX functional (black) and GGA + U methods (red), with U value of 9.5 eV on F-p orbitals. The total DOS of bulk CaF_2 is shaded in (a) right panel. VBM is set at energy zero.

(12.1 eV for the direct gap and 11.8 eV for the indirect gap).[34] The top VB states remain the same in their structure and the valence bandwidth is slightly increased from 2.64 eV in LDA to 2.75 eV in sX, improving the compressed VB reported in the previous work.[11] The dispersion of the CB is greatly modified, with the CBM at Γ 1.35 eV lower than the X_1 state, which is similar to former GW results.[7]

Different U value combinations are tested on Ca d and F p orbitals. The U parameters are selected by minimizing the error between the calculated GGA + U and sX band energies for VB and CB states[16] at high symmetry points L, Γ, and X. The calculated results show that the addition of U on Ca d states has a negative effect on the bandgap value while adding U to the F p states could effectively open up the gap. The bandgap of CaF_2 can be corrected using the GGA + U method to properly agree with the sX results of 11.78 eV by adding 9.5 eV on F-2p states [Fig. 1(b)]. Both the top VB and bottom CB retain the GGA band structure, with the valence and conduction bandwidths being stretched to 3.60 and 3.46 eV, respectively.

B. Band alignment at the CaF_2/Si interface

We note that different methods can position the band edges differently even when they give the same bandgap values. This phenomenon can directly affect the prediction of heterostructure band offsets. So we also consider the ionization potential (IP) of bulk cubic CaF_2 using a non-polar (110) CaF_2 slab with a thick vacuum layer to validate the GGA + U method in an absolute energy scale. Overall, the results calculated by the GGA + U method are all in good agreement with the sX calculations as well as the experimental values. The accurate prediction of IP values by the GGA + U method is similar to the case of MgO[17] and supercedes the case of HfO_2.[16]

For the CaF_2/Si(111) interface, we adopt the T_4 configuration with B-type orientation along the z-direction as shown in Fig. 2(a). The interface is charge neutral, and the Ca atoms are located at the high symmetry T_4 sites while the F atoms are in H_3 sites of the Si (111)-(1 × 1) surface. The validity of such interface morphology has been extensively justified experimentally.[21,36] Furthermore, theoretical works based on this model are shown to reproduce the experimentally measured band alignment.[8] In the case of Si, our calculation with GGA functional gives an indirect bandgap of 0.68 eV. Although smaller than the experimental bandgap data (1.17 eV), the difference is acceptable compared to the large gap

TABLE I. Band energies and IP values for CaF_2, calculated by GGA, GGA + U, and sX methods, compared to experimental data. The positions of the lowest CB (c) and the highest VB (v) at high-symmetry points are studied. The uppermost VB at X is set at energy zero.

		L_{3c}	L'_{3v}	Γ_{1c}	Γ_{15v}	X_{1c}	X'_{2v}	Minimum gap (X–Γ)	EA	IP
GGA		9.23	−0.77	7.11	−0.28	8.05	0.00	7.11	−0.30	6.81
GGA + U		12.70	−1.07	11.11	−0.34	11.57	0.00	11.11	−0.39	10.71
sX		15.05	−0.86	11.78	−0.24	13.13	0.00	11.78	−0.22	11.55
Exp.	34			…				11.80	…	…
	35			…				12.11	−0.15	11.96

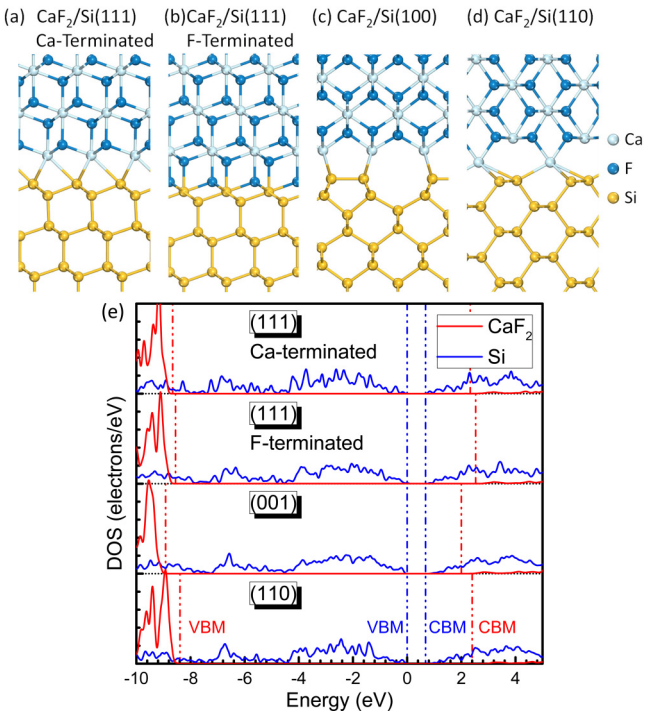

FIG. 2. Atomic structures of (a) (111), (b) (001), and (c) (110) CaF_2/Si interfaces, respectively. The PDOS of the three orientations is shown in (d). The PDOS is obtained from bulk layers that are away from the interfacial region. The VBM of Si bulk is set to energy zero.

value of CaF_2, since we are more interested in the band offset values at the CaF_2/Si interface. Evidence for Si–F bonds formed at the interface has also been established.[20] Accordingly, we considered various F-terminated interface models, and the most structurally stable configuration has two interfacial fluorine layers with F sitting at the hollow sites of the first-layer Si atoms with A-type orientation, as shown in Fig. 2(b).

Previous works found that the lattice orientation of CaF_2 deposited onto Si(001) mimics the orientation of the substrate when the growth is performed at a temperature below 600 °C.[37] The atomic force microscopy (AFM) images together with reflection high-energy electron diffraction (RHEED) results indicate that the Si(001) surface is reconstructed in the form of dimer rows and gives rise to 2×1 periodicity. On the other hand, the formation of the interfacial Ca–Si bond is supported by photoemission.[37] Based on the existing experiment data, we propose a 2×1 reconstructed interface composed of fivefold Si sites with lateral Si–Si bonds and Ca on top of the second-layer Si atoms [Fig. 2(b)], using the basic ideas of the well-understood sevenfold model for the silicide/Si(001) interface.[38,39]

The present reports are not conclusive about the detailed atomic geometry at CaF_2/Si(110). We build the model with CaF_2(110)||Si(110) and CaF_2[110]||Si[110]. However, the direct contact between ideal (110) faces of CaF_2 and Si is not an insulating interface because there are now states within the bandgap. CaF_2 has ionic bonding without a fixed coordination like ZrO_2, and the (110) face of CaF_2 is neutral,[40] while the Si(110) face has one half-filled dangling bond (DB) per surface Si atom. To accommodate the extra electrons donated by Si and create an insulating interface, we remove all F atoms at the first CaF_2 layer to satisfy the electron counting rule,[40] forming a Ca-terminated interface with fivefold coordinated Ca as shown in Fig. 2(c).

The local DOSs of Si and CaF_2 presented in Fig. 2(d) clearly show that all the interfacial models are insulating without any gap states in the bandgap, so our models all perfectly satisfy the electron counting. This is the basis of the accurate analysis of the band alignment data.

Figure 3 shows the extracted band offset values by the core-level scheme. All three Ca-terminated interfaces exhibit obvious type-II band alignment. The calculated valence band offsets (VBOs) ΔE_V of (111), (001), and (110) orientations are 8.66, 8.92, and 8.39 eV, respectively. The substrate orientation affects the band alignment and shows a relation of $\Delta E_V(001) > \Delta E_V(111) > \Delta E_V(110)$ with a corresponding inverse conduction band offsets (CBOs) trend.

It is useful to compare the present results with the available experimental and theoretical data. The experimental VBOs for the Si/CaF_2(111) range from 8.5 to 8.9 eV,[23–25] while the hybrid functional-like PBE0, HSE, and GW methods considered in the former theoretical work deduced VBOs from 8.28 to 9.01 eV.[8] Our GGA + U results yield a reasonable agreement with existing results showing errors of at most ~0.4 eV.

To quantitatively characterize the electronic charge distribution at different interfaces and, hence, to explain the VBO variation, we perform the Mulliken atomic population analysis. Figure 4 summarizes the gross atomic charges by the Mulliken analysis at individual layers from the interface model. Note that since we remove interfacial F atoms at the (110) interface, the F starts counting from the second layer in the Si/CaF_2(110) case.

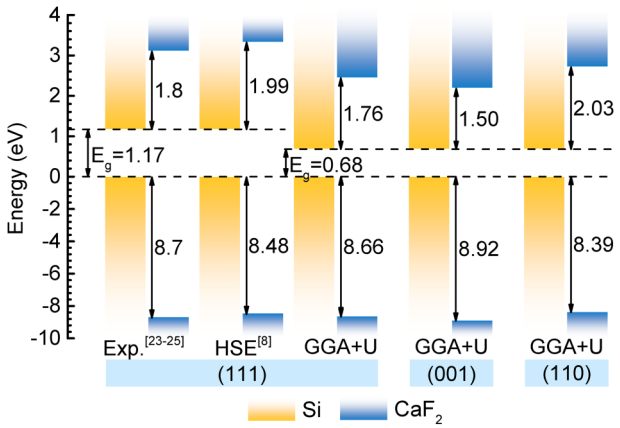

FIG. 3. Energy band alignment diagram of Ca-terminated (111)-, (001)-, and (110)-oriented interfaces. Experimental data[23–25] and previous HSE calculations[8] are given for comparison. The CBOs of the reference data are based on VBOs and the experimental bandgap of 11.8 eV in Ref. 8.

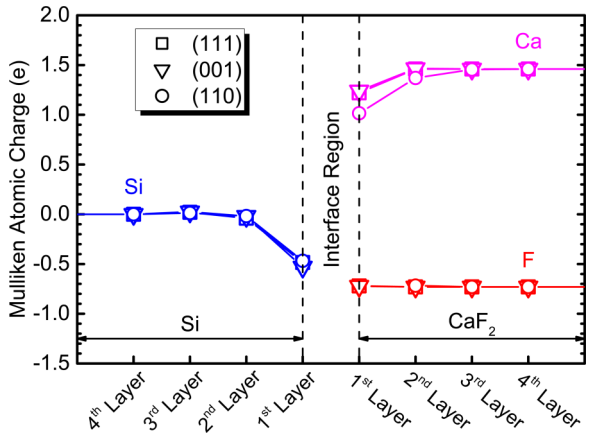

FIG. 4. Mulliken atomic charge for Si, Ca, and F atoms in individual layers, where the positive (negative) charge means electron depletion (accumulation). The interface region is labeled to separate the two sides.

The Ca atoms carry positive charge and the F atoms are negatively charged. Electron accumulation is also investigated on interfacial Si atoms.

The results indicate that the charge transfer between CaF_2 and Si is limited at the interface region, with only the Ca and Si atoms being involved. The interfacial effect deteriorates dramatically and reproduces the bulk charge population distribution from the third layer of CaF_2 and Si. The charge transfer from Ca to Si leads to dipole formation at the interface, which shifts the energy position of the CaF_2 VBM upward with respect to the Si VBM, thus reducing the VBO of the (110) interface. At the Si/CaF_2(110) interface, the Ca:Si ratio is 1:2, and the charge transfer to the first Si layer per Ca atom is 0.93e. The Ca:Si ratios under the other two conditions are equal to 1, and the charge transfer of the (111) and (001) orientations are 0.72e and 0.53e, respectively. The amount of charge transfer suggests the strength of the dipole. The (110)-oriented interface with the most pronounced charge rearrangement, therefore, has the smallest VBO.

C. SBHs at the metal/CaF_2 interface

We study the metal/CaF_2 interfaces to verify the Fermi-level pinning character as well as testing the calculation convergence. The F^- terminated polar (111) and (001) as well as the non-polar (110) surfaces are studied with different metals covering a wide work function range from 3.5 eV (Sc) to 5.6 eV (Pt).[41] Six layers of metals in their FCC structure and ~20 Å of CaF_2 are used to construct the model. The SBHs are extracted using the core-level method. Although terminated with F^- ions, the (111) face of CaF_2 can be considered as $F^-Ca^{2+}F^-$ trilayers stacking along [111].[40] The nonpolar $F^-Ca^{2+}F^-$ unit yields a closed-shell configuration, so the (111) termination is stable [Fig. 5(a)]. We now transfer the same idea to the F-terminated (001) surface, so half of the F^- ions in one layer are equally distributed to the Ca^{2+} ions at both sides, which leave extra F^- ions at the surface. We, thus, remove half of the F atoms at the interface model to reach stable termination, as shown in Fig. 5(b). The non-polar (110) surface is left intact [Fig. 5(c)].

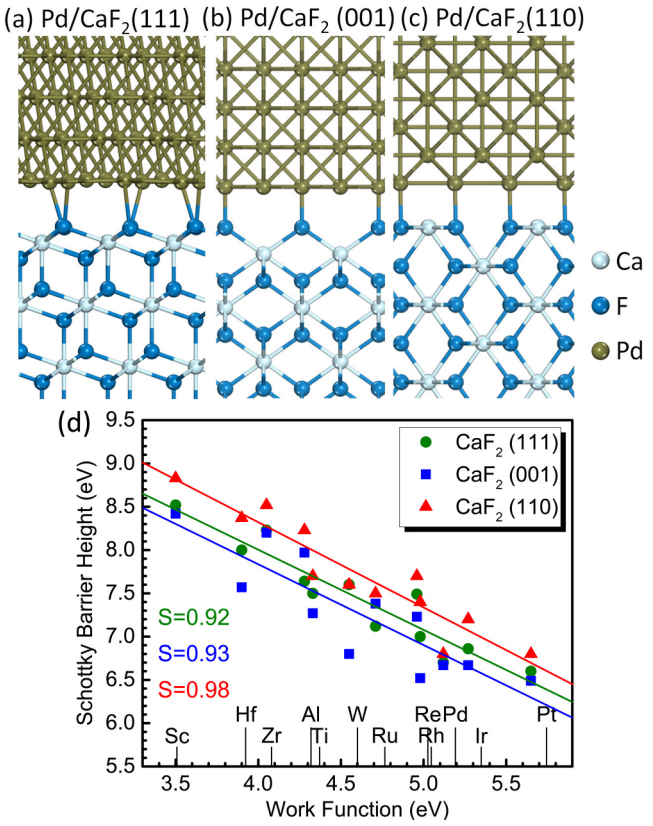

FIG. 5. Interface models for CaF_2 (a) (111), (b) (001), and (c) (110) interfaces with contact metal of Pd. The calculated p-type SBHs of various metals on different terminations of CaF_2 are in (d). Work function values are from Ref. 41.

The SBHs are extracted from interface calculations as summarized in Fig. 5(d). We find that there is a linear dependence of SBH on the metal work function. The pinning factor S is calculated by the fitted slope and is found to be ~0.9 for each orientations, indicating weakly pinned interfaces approaching the Schottky limit.[30] This S value is consistent with the highly ionic nature of CaF_2,[28] and it matches the empirical value predicted by the metal-induced gap state (MIGS) model ($S = 0.89$),

$$S = \frac{1}{1 + 0.1(\varepsilon_\infty - 1)^2}, \tag{3}$$

where ε_∞ is the optical dielectric constant.[29,30] We also note that there are different offsets for different terminations. From (110) to (111), there is a downward shift of ~0.4 eV in SBHs, and a further ~0.1 eV decrease is observed from (111) to (001) interface.

IV. CONCLUSION

In summary, the CaF_2 band structure is studied in detail with different calculation methods. Both sX and GGA + U results show good agreement with the experiments and previous theoretical works. Further calculations are performed with the GGA + U method to systematically study the band offsets of CaF_2/Si and SBHs of metal/CaF_2 interfaces. It is found that the GGA + U can effectively reproduce the experimental bandgap, with the U term added only on the anion-p states. The band offsets calculated by GGA + U satisfactorily match the experimental values and the advanced electronic structure results. We also show the band offsets to follow a relation of $\Delta E_V(001) > \Delta E_V(111) > \Delta E_V(110)$, which could be explained by the dipole formation at the interface. Furthermore, we study the metal/CaF_2 interfaces and find that metal contacts on CaF_2 are weakly pinned, leading to the Schottky limit. The accurate description of CaF_2 band energies indicates the accuracy of sX in treating the large gap materials. Meanwhile, the replication of the experimental results regarding interface properties with the GGA + U scheme proves that we can achieve fast yet faithful calculations of electronic structures of solids with this approach in the case of fluorides like CaF_2.

ACKNOWLEDGMENTS

The authors acknowledge funding from EPSRC under Grant No. EP/P005152/1. We also thank support from Cambridge CSD3 Supercomputing under Project No. CS129 and Supercomputing Wales under Project No. SCW1070.

AUTHOR DECLARATIONS

Conflicts of Interest

The authors have no conflicts to disclose.

DATA AVAILABILITY

The data that support the findings of this study are available from the corresponding author upon reasonable request.

REFERENCES

[1]G. Wang, Q. Peng, and Y. Li, J. Am. Chem. Soc. **131**, 14200 (2009).
[2]Y. Y. Illarionov, A. G. Banshchikov, D. K. Polyushkin, S. Wachter, T. Knobloch, M. Thesberg, M. I. Vexler, M. Waltl, M. Lanza, N. S. Sokolov, T. Mueller, and T. Grasser, 2D Mater. **6**, 045004 (2019);Y. Y. Illarionov, A. G. Banshchikov, D. K. Polyushkin, S. Wachter, T. Knobloch, M. Thesberg, L. Mennel, M. Paur, M. Stöger-Pollach, A. Steiger-Thirsfeld, M. I. Vexler, M. Waltl, N. S. Sokolov, T. Mueller, and T. Grasser, Nat. Electron. **2**, 230 (2019);C. Wen and M. Lanza, Appl. Phys. Rev. **8**, 021307 (2021).
[3]L. Sang, M. Liao, Y. Koide, and M. Sumiya, Appl. Phys. Lett. **98**, 103502 (2011).
[4]Z. Zhang, Y. Guo, H. Lu, S. J. Clark, and J. Robertson, Appl. Phys. Lett. **116**, 131602 (2020).
[5]A. Schleife, C. Rödl, F. Fuchs, J. Furthmüller, and F. Bechstedt, Phys. Rev. B **80**, 035112 (2009).
[6]M. Verstraete and X. Gonze, Phys. Rev. B **68**, 195123 (2003).
[7]Y. Ma and M. Rohlfing, Phys. Rev. B **75**, 205114 (2007).
[8]T. Bischoff, I. Reshetnyak, and A. Pasquarello, Phys. Rev. B **101**, 235302 (2020).
[9]S. J. Clark and J. Robertson, Phys. Rev. B **82**, 085208 (2010).
[10]J. Heyd, G. E. Scuseria, and M. Ernzerhof, J. Chem. Phys. **118**, 8207 (2003).
[11]M. Kim, Y.-J. Zhao, A. J. Freeman, and W. Mannstadt, Appl. Phys. Lett. **84**, 3579 (2004).
[12]S. J. Clark, T. W. Hollins, K. Refson, and N. I. Gidopoulos, J. Phys.: Condens. Matter **29**, 374002 (2017).
[13]V. I. Anisimov, J. Zaanen, and O. K. Andersen, Phys. Rev. B **44**, 943 (1991).
[14]A. Janotti, D. Segev, and C. G. Van de Walle, Phys. Rev. B **74**, 045202 (2006).
[15]D. O. Scanlon, B. J. Morgan, and G. W. Watson, J. Chem. Phys. **131**, 124703 (2009).
[16]Y. Guo, Z. Zhang, and J. Robertson, Phys. Status Solidi RRL **15**, 2100295 (2021).
[17]J. Chen, Z. Zhang, Y. Guo, and J. Robertson, J. Appl. Phys. **129**, 175304 (2021).
[18]Y. Guo, H. Li, S. J. Clark, and J. Robertson, J. Phys. Chem. C **123**, 5562 (2019).
[19]Y. Y. Illarionov, M. I. Vexler, V. V. Fedorov, S. M. Suturin, and N. S. Sokolov, J. Appl. Phys. **115**, 223706 (2014);C. Wen, A. G. Banshchikov, Y. Y. Illarionov, W. Frammelsberger, T. Knobloch, F. Hui, N. S. Sokolov, T. Grasser, and M. Lanza, Adv. Mater. **32**, 2002525 (2020).
[20]M. A. Olmstead, R. I. G. Uhrberg, R. D. Bringans, and R. Z. Bachrach, Phys. Rev. B **35**, 7526 (1987).
[21]R. M. Tromp and M. C. Reuter, Phys. Rev. Lett. **61**, 1756 (1988).
[22]J. D. Denlinger, E. Rotenberg, U. Hessinger, M. Leskovar, and M. A. Olmstead, Phys. Rev. B **51**, 5352 (1995).
[23]F. J. Himpsel, U. O. Karlsson, J. F. Morar, D. Rieger, and J. A. Yarmoff, Phys. Rev. Lett. **56**, 1497 (1986).
[24]D. Rieger, F. J. Himpsel, U. O. Karlsson, F. R. McFeely, J. F. Morar, and J. A. Yarmoff, Phys. Rev. B **34**, 7295 (1986).
[25]A. Izumi, Y. Hirai, K. Tsutsui, and N. S. Sokolov, Appl. Phys. Lett. **67**, 2792 (1995).
[26]E. Rotenberg, J. D. Denlinger, M. Leskovar, U. Hessinger, and M. A. Olmstead, Phys. Rev. B **50**, 11052 (1994).
[27]E. Rotenberg, J. D. Denlinger, and M. A. Olmstead, Phys. Rev. B **53**, 1584 (1996).
[28]M. Dixon and M. J. Gillan, J. Phys. C: Solid State Phys. **11**, L165 (1978).
[29]J. Tersoff, Phys. Rev. Lett. **52**, 465 (1984); W. Mönch, Phys. Rev. Lett. **58**, 1260 (1987).
[30]J. Robertson, J. Vac. Sci. Technol. B **18**, 1785 (2000).
[31]S. J. Clark, M. D. Segall, C. J. Pickard, P. J. Hasnip, M. I. J. Probert, K. Refson, and M. C. Payne, Z. Kristallogr. Cryst. Mater. **220**, 567 (2005).
[32]E. A. Kraut, R. W. Grant, J. R. Waldrop, and S. P. Kowalczyk, Phys. Rev. Lett. **44**, 1620 (1980).
[33]Z. Zhang, Y. Guo, and J. Robertson, Appl. Phys. Lett. **114**, 161601 (2019).
[34]G. W. Rubloff, Phys. Rev. B **5**, 662 (1972).
[35]R. T. Poole, D. R. Williams, J. D. Riley, J. G. Jenkin, J. Liesegang, and R. C. G. Leckey, Chem. Phys. Lett. **36**, 401 (1975).
[36]C. Deiter, M. Bierkandt, A. Klust, C. Kumpf, Y. Su, O. Bunk, R. Feidenhans'l, and J. Wollschläger, Phys. Rev. B **82**, 085449 (2010).
[37]L. Pasquali, S. M. Suturin, V. P. Ulin, N. S. Sokolov, G. Selvaggi, A. Giglia, N. Mahne, M. Pedio, and S. Nannarone, Phys. Rev. B **72**, 045448 (2005).
[38]B. D. Yu, Y. Miyamoto, O. Sugino, A. Sakai, T. Sasaki, and T. Ohno, J. Vac. Sci. Technol. B **19**, 1180 (2001).
[39]U. Falke, A. Bleloch, M. Falke, and S. Teichert, Phys. Rev. Lett. **92**, 116103 (2004);Z. Zhang, Y. Guo, and J. Robertson, J. Phys. Chem. C **124**, 19698 (2020).
[40]P. W. Peacock and J. Robertson, Phys. Rev. Lett. **92**, 057601 (2004).
[41]H. B. Michaelson, J. Appl. Phys. **48**, 4729 (1977).